Prion strain discrimination using luminescent conjugated polymers

Christina J Sigurdson[1,6], K Peter R Nilsson[1,6], Simone Hornemann[2], Giuseppe Manco[1], Magdalini Polymenidou[1], Petra Schwarz[1], Mario Leclerc[3], Per Hammarström[4], Kurt Wüthrich[2,5] & Adriano Aguzzi[1]

The occurrence of multiple strains of prions may reflect conformational variability of PrP^{Sc}, a disease-associated, aggregated variant of the cellular prion protein, PrP^{C}. Here we used luminescent conjugated polymers (LCPs), which emit conformation-dependent fluorescence spectra, for characterizing prion strains. LCP reactivity and emission spectra of brain sections discriminated among four immunohistochemically indistinguishable, serially mouse-passaged prion strains derived from sheep scrapie, chronic wasting disease (CWD), bovine spongiform encephalopathy (BSE), and mouse-adapted Rocky Mountain Laboratory scrapie prions. Furthermore, using LCPs we differentiated between field isolates of BSE and bovine amyloidotic spongiform encephalopathy, and identified noncongophilic deposits in prion-infected deer and sheep. We found that fibrils with distinct morphologies generated from chemically identical recombinant PrP yielded unique LCP spectra, suggesting that spectral characteristic differences resulted from distinct supramolecular PrP structures. LCPs may help to detect structural differences among discrete protein aggregates and to link protein conformational features with disease phenotypes.

According to the protein-only hypothesis[1] prions are composed solely of PrP^{Sc} and can give rise to multiple distinct strains that elicit transmissible spongiform encephalopathy (TSE) with different incubation periods and lesion profiles—even after serial transmission through congenic hosts sharing the same PrP sequence. Because prion strains may vary in their transmissibility to humans, strain discrimination is of keen interest for prion diagnostics and for public health. Prion strains had been originally distinguished by characteristic incubation periods in differentially susceptible inbred mice[2]. Strains may also differ in their capability of inducing morphologically diverse aggregates and amyloid plaques, and they can target different brain regions[3,4]. PrP^{Sc} from distinct prion strains can differ in electrophoretic mobility[5], immunological reactivity to amino-proximal antibodies upon proteinase K digestion[6] and relative glycoform ratio[7]. Finally, the PrP^{Sc}-capturing efficacy of conformational antibodies[8] and the stability of PrP^{Sc} to chaotropes[9] have been shown to be strain-dependent. Overall, this suggests that the tertiary and/or quaternary structure of PrP^{Sc} aggregates might define prion strains[10]. Alternative explanations include, for example, differential binding of PrP^{Sc} from distinct strains to additional components, some of which may not even be proteins[11].

Here we report the use of LCPs to biophysically characterize prion protein aggregates with distinct biochemical and histopathological properties, which are indicative of specific prion strain isolates. In contrast to sterically rigid amyloidotropic dyes such as thioflavin T and Congo red, the LCPs used in this work contain swiveling thiophene backbones whose geometry modulates their fluorescence. Noncovalent binding to proteins, including amyloids[12,13], constrains the rotational freedom of LCPs and thus alters their spectral properties in a conformation-dependent manner[14,15]. Histochemical LCP stains may therefore yield a sensitive method for detecting conformational variability in prion and other amyloidogenic protein aggregates.

We tested a library of LCPs with distinct ionic side chains, and used the spectral properties of a given LCP bound to different PrP aggregates to distinguish a variety of laboratory mouse and natural prion strains. This method demonstrates that the LCPs can be used to gain direct insight into the structural variability between different misfolded proteins.

RESULTS

Creation of prion strains

We created several distinct prion strains by preparing prion inocula from various ruminants and transmitting them to PrP^{C}-overexpressing tga20 transgenic mice[16] and to wild-type C57BL/6 mice. We intracerebrally inoculated tga20 mice ($n = 4$–10) with brain homogenates derived from a mule deer naturally infected with CWD, a naturally scrapie-infected (NS) Suffolk sheep from Colorado, a BSE-infected cow and the mouse-adapted Rocky Mountain Laboratory (RML) scrapie strain, resulting in

[1]UniversitätsSpital Zürich, Institute of Neuropathology, Department of Pathology, Schmelzbergstrasse 12, CH–8091 Zürich, Switzerland. [2]Institut für Molekularbiologie und Biophysik, ETH Zürich, CH-8093 Zürich, Switzerland. [3]Department of Chemistry, Vachon Building, Rue de la Médecine, Université Laval, Quebec City, G1K 7P4, Canada. [4]Department of Chemistry, Linköping University, 581 83 Linköping, Sweden. [5]Department of Molecular Biology and Skaggs Institute for Chemical Biology, The Scripps Research Institute, La Jolla, California 92037, USA. [6]These authors contributed equally to this work. Correspondence should be addressed to A.A. (adriano.aguzzi@usz.ch).

RECEIVED 31 JULY; ACCEPTED 19 OCTOBER; PUBLISHED ONLINE 18 NOVEMBER 2007; DOI:10.1038/NMETH1131

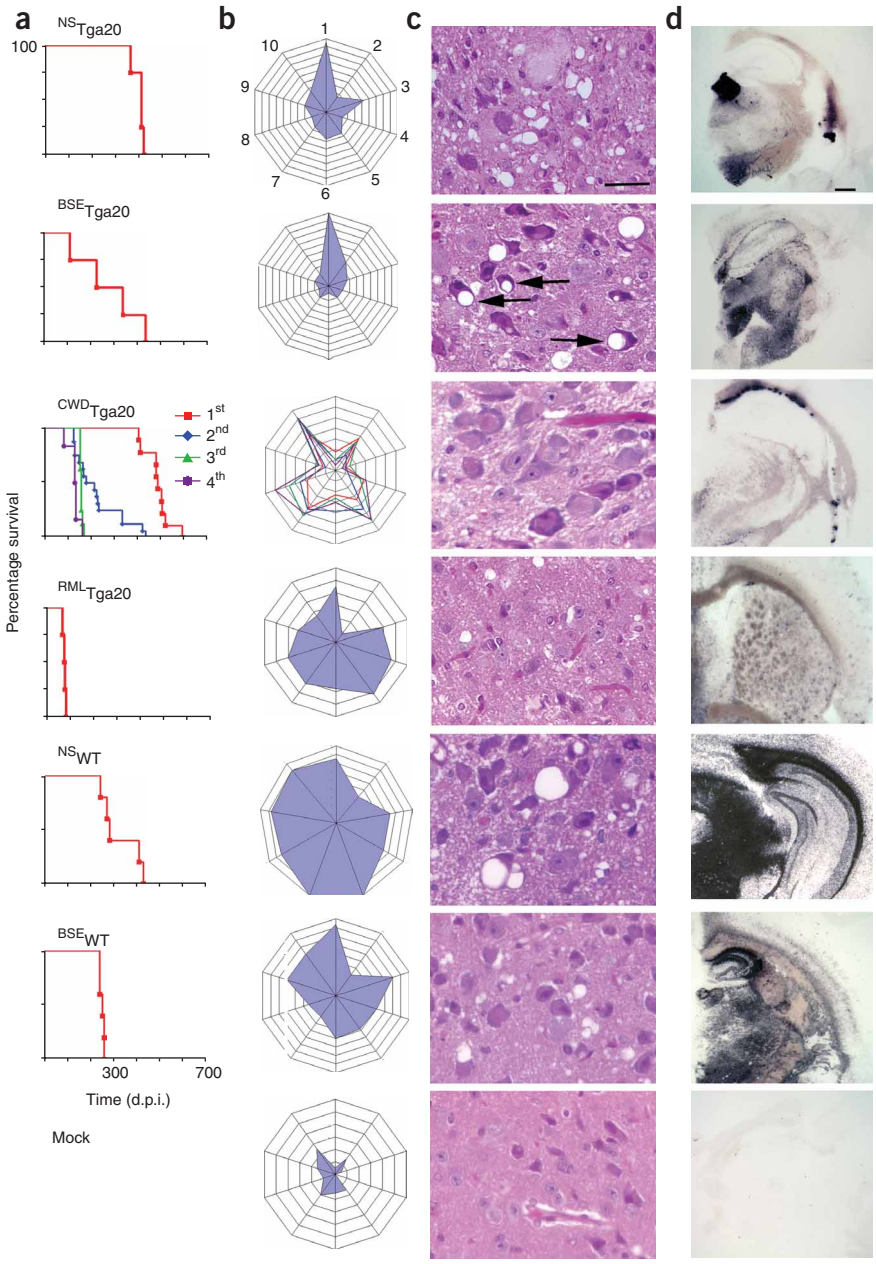

Figure 1 | Disease phenotypes generated with four prion strains in tga20 and wild-type mice. (**a**) Survival period of the mice used to obtain the data shown in **b**–**d** (d.p.i., days post-inoculation). (**b**) Histopathological lesion severity score (astrogliosis, spongiform change and PrP^{Sc} deposition) in 10 regions of brain (see Methods). Each ring represents one point. (**c**) Brainstem pathology assayed by hematoxylin and eosin staining. The arrows indicate large intracellular vacuoles in BSE-inoculated mice. (**d**) Histological blots illustrating patterns of spongiosis and PrP^{Sc} deposition with PrP antibody SAF84. Scale bars, 50 μm (**c**) and 500 μm (**d**).

diseased ^{CWD}tga20, ^{NS}tga20, ^{BSE}tga20 and ^{RML}tga20 mice. We passaged brain homogenates from sick ^{CWD}tga20 mice three more times to tga20 mice[17], and we passaged brain homogenates from sick ^{BSE}tga20 and ^{NS}tga20 into wild-type mice to create ^{BSE}WT and ^{NS}WT (**Fig. 1**).

All ^{BSE}tga20, ^{BSE}WT, ^{NS}tga20, ^{NS}WT, multiply passaged ^{CWD}tga20 and ^{RML}tga20 mice displayed spongiform change and PrP^{Sc} deposition (**Fig. 1c,d** and **Supplementary Fig. 1** online). Morphometric analysis of spongiosis, gliosis and PrP deposition in eight standardized regions of gray matter and two regions of white matter[18] revealed superimposable lesion profiles for ^{NS}tga20 and ^{BSE}tga20, which were, however, distinct from those of ^{CWD}tga20 brains (**Fig. 1b**). Individual mouse prion isolates also exhibited unique biochemical properties when probed by conformational stability assay, glycoform profile and the core fragment size of PrP^{Sc} (**Supplementary Figs. 1** and **2** online). All of the above suggests that these mouse-adapted TSEs differ in properties that are intrinsic to the infectious agent and that the murine TSE isolates represent distinct prion strains.

Staining of formalin-fixed brain sections

We next characterized PrP aggregates in formic acid–treated, formalin-fixed paraffin-embedded brain tissue sections from the TSE-infected mice, using several fluorescent dyes and a PrP antibody (SAF84; SPI BIO). To first determine which PrP^{Sc} deposits would formally qualify as amyloid, we stained the brain sections with Congo red (**Fig. 2** and **Supplementary Fig. 3** online). ^{CWD}tga20, ^{NS}tga20 and a subset of ^{BSE}WT plaques were congophilic. We then exposed brain tissue sections to the LCPs polythiophene acetic acid (PTAA)[19] or polythiophene methyl imidazole (PTMI)[20] (**Fig. 2a**). Upon staining with PTAA (anionic at pH = 10.2), ^{CWD}tga20, ^{NS}tga20, ^{NS}WT and the congophilic subset of ^{BSE}WT plaques fluoresced very brightly, whereas we visualized no deposits in ^{RML}tga20 and ^{BSE}tga20 brains (**Fig. 2b** and **Supplementary Fig. 3a**). By comparison, PTMI (cationic at pH = 1.6) stained all PrP aggregates except ^{BSE}tga20 and ^{NS}WT (**Fig. 2b**). Hence, LCPs identify noncongophilic PrP aggregates in addition to congophilic plaques. However, ^{BSE}tga20 was not stained by either probe. Taken together, these results show that the LCPs, with their distinctive ionic side chains, selectively bind to PrP aggregates of particular prion strains.

Colocalization of plaques by PrP-antibody SAF84 and PTAA indicated that PTAA specifically stains PrP aggregates (**Fig. 2b**). We observed light nuclear and background fluorescence both in PTAA and in antibody-stained sections. When we used a long-pass filter (LP470; Zeiss) to collect a broad emission profile (**Fig. 2c**), emission spectra from nuclei and background were blue-shifted compared to the spectrum from PTAA-bound PrP^{Sc} plaques (**Fig. 2d**). The fluorescence from entities other than PrP aggregates might arise from the formic acid treatment and formalin fixation or represent weak PTAA staining. To unambiguously discriminate nuclei, background and PrP aggregates, we performed spectral

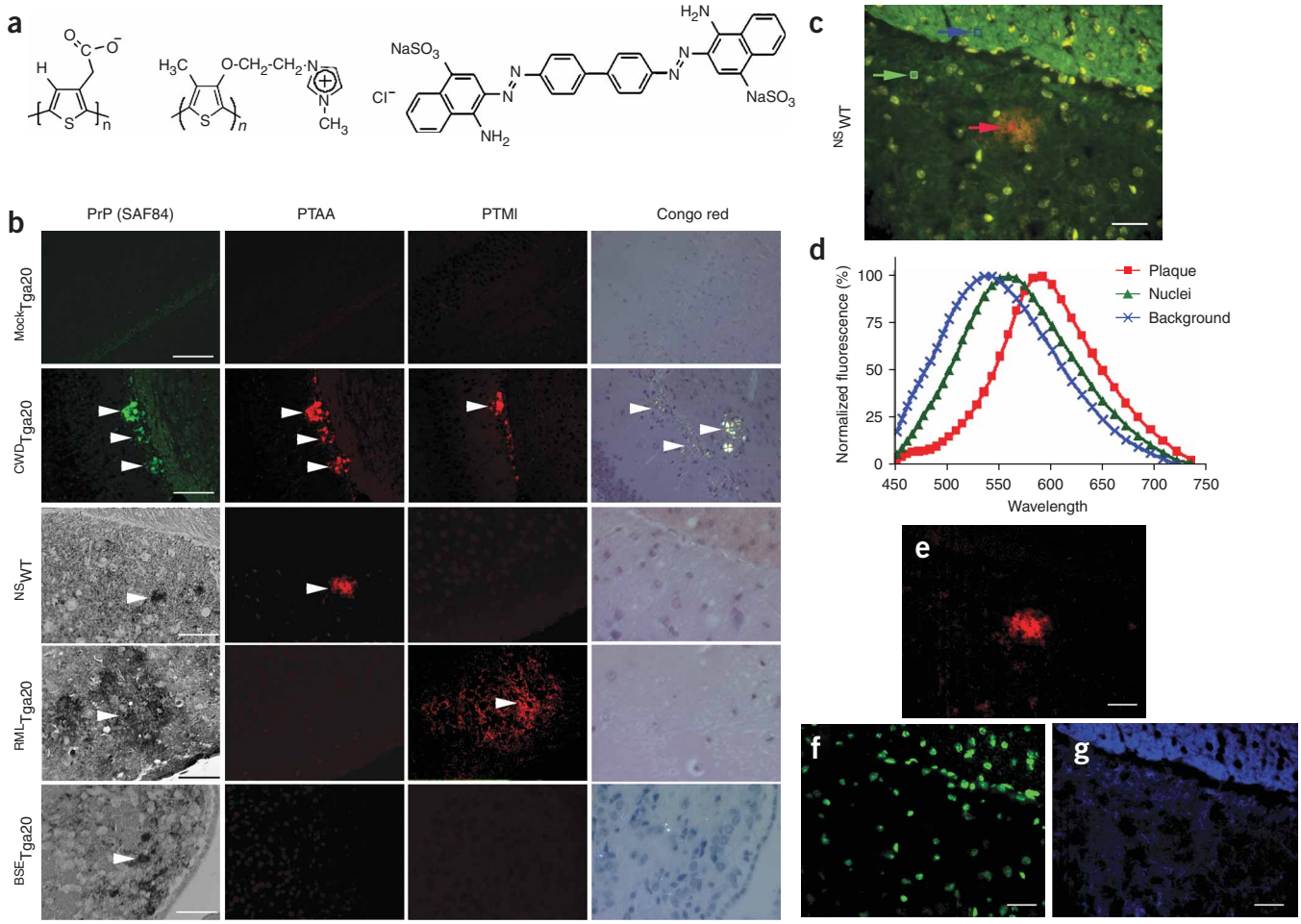

Figure 2 | LCP staining patterns distinguish prion strains in mouse formalin-fixed brain sections. (**a**) Structures of PTAA (left), PTMI (middle) and Congo red (right). (**b**) Fluorescence images showing SAF84, PTAA, PTMI and Congo red staining of ^{mock}tga20 control brain, ^{CWD}tga20, ^{NS}WT, ^{RML}tga20 and ^{BSE}tga20 brains. Both PTAA and PTMI stained the congophilic PrP aggregates observed in ^{CWD}tga20. Additionally, PTAA stained the noncongophilic PrP aggregates in ^{NS}WT, whereas PTMI stained the PrP-aggregates in ^{RML}tga20. LCPs did not stain ^{BSE}tga20 aggregates. Arrowheads indicate PrP aggregates. (**c**) ^{NS}WT brain stained by PTAA. (**d**) Spectra collected from the plaque, nuclei and background, recorded at the positions of the three squares in **c** (marked by arrows). (**e**–**g**) The same microscopy field as in **c**, analyzed by spectral unmixing, which shows all pixels with the same spectrum as that of the square within the plaque in **c** (**e**), from a nucleus (**f**) or from the background (**g**). Scale bars, 100 μm (**b**, mock and CWD), 50 μm (**b**, NS, RML and BSE) and 20 μm (**c**–**g**).

unmixing, whereby pixels from a particular structure are selected, and all spectral profiles within a visual field that match the selected region are highlighted (**Fig. 2e–g**). We could easily identify PrP aggregates owing to the specific emission profile from PTAA. Mock-inoculated mouse brains (n = 10) did not show any appreciable signal with any of the LCPs (**Fig. 2b**). The cationic and zwittierionic LCPs, POMT and PONT, respectively, which had previously been reported to stain amyloid plaques[13], showed staining identical to Congo red (data not shown).

Staining of brain tissue cryosections

Because formic acid treatment and formalin fixation tend to disrupt the native structure of the prion aggregates, we characterized native-like PrP aggregates in brain cryosections from TSE-infected mice. To avoid uncontrolled perturbations of the tertiary and/or quaternary structure of PrP^{Sc}, we shock-froze the tissues in liquid nitrogen and fixed the cryostat sections in ethanol. The LCP staining pattern was identical to the results obtained from the paraffin brain sections. In addition, when stained with PTAA, the thioflavin T^+ congophilic plaques emitted strikingly different hues of light (**Fig. 3a**). Upon excitation at 488 nm, ^{CWD}tga20 plaques displayed a greenish spectrum with the emission maximum (E_{max}) around 565 nm, whereas ^{BSE}WT and ^{NS}tga20 plaques emitted red-shifted spectra (E_{max} = 585 nm; **Fig. 3b**). These emission spectra indicated conformational changes in the LCP. Twisted, separated LCP chains fluoresce in green (532 nm), whereas a planar arrangement of the LCP backbone leads to progressive red-shift toward longer wavelengths for E_{max}. Fluorescence at 639 nm results from intermolecular energy transfer between closely spaced LCP molecules[21–23].

We could clearly distinguish the three prion strains, ^{CWD}tga20, ^{BSE}WT and ^{NS}tga20, by using a correlation diagram of the ratios of fluorescence intensities at specific wavelengths, $R_{532/639}$ and $R_{532/Emax}$, as an indicator of the conformation of plaque-bound PTAA (**Fig. 4a**,**b** and **Supplementary Tables 1** and **2** online). The emission spectrum of ^{CWD}tga20 plaques ($R_{532/639}$: 1.55 ± 0.10; $R_{532/Emax}$: 0.92 ± 0.03) indicates a nonplanar, separated state of PTAA. The spectra of ^{NS}tga20 and ^{BSE}WT plaques suggest tight stacking and a more planar backbone of PTAA (**Figs. 3b** and **4a**,

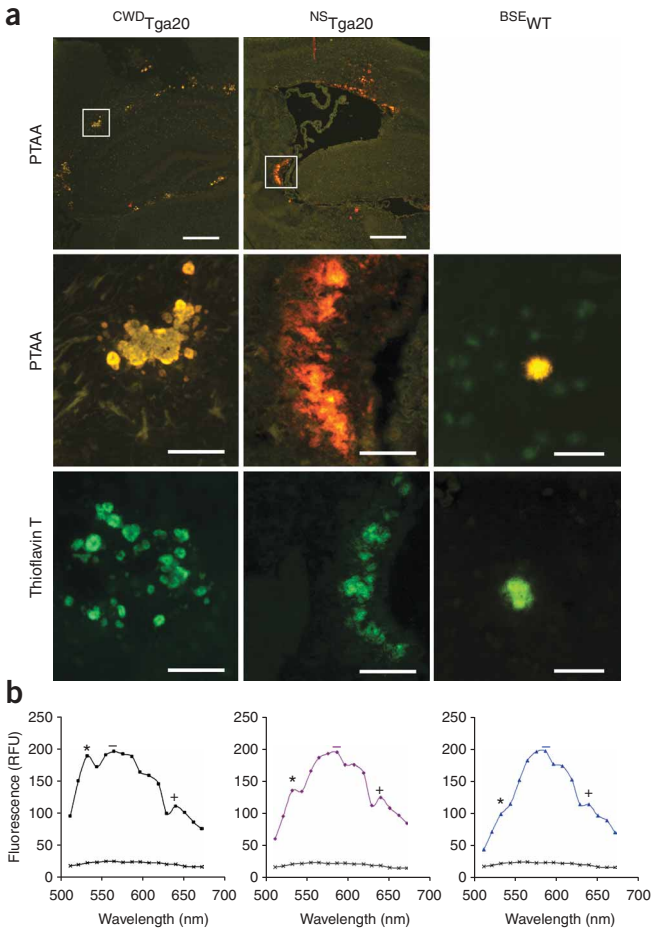

Figure 3 | PTAA and thioflavin T staining of PrP deposits in prion-infected brain cryosections. (**a**) Images showing PTAA and thioflavin T bound to PrP aggregates from ^{CWD}tga20, ^{NS}tga20 and some ^{BSE}WT. To show the localization and the selective staining of the PrP aggregates, low and high magnifications of the boxed regions are shown for ^{CWD}tga20 and ^{NS}tga20. (**b**) Spectra of PTAA bound to ^{CWD}tga20 (black), ^{NS}tga20 (purple) and ^{BSE}WT (blue) deposits. –, E_{max}; *, $E_{532\ nm}$; +, $E_{639\ nm}$. Background signal, black line. Scale bars, 500 μm (**a**; PTAA, top), 50 μm (**a**; PTAA, middle, and thioflavin T).

and **Supplementary Tables 1** and **2**). Hence the spectral signatures of PTAA-stained PrP aggregates in mouse brains reliably discriminate between prions originating from scrapie-infected sheep, BSE-infected cattle or CWD-infected cervids.

We then analyzed the spectra of serially passaged ^{CWD}tga20 mice and observed progressive PTAA spectral changes over four passages, with spectra illustrating a gradual change toward higher planarity and aggregation. This indicates that PTAA can precisely track subtle phenomena occurring during prion strain adaptation in mouse hosts (**Fig. 4b**, and **Supplementary Tables 2** and **3** online). We also assessed first and second passages of sheep scrapie in ^{NS}tga20 and ^{NS}WT mice. PTAA stained both noncongophilic ^{NS}WT and congophilic ^{NS}tga20 plaques and emitted nearly identical spectra (**Fig. 4a**).

Staining of recombinant PrP fibrils

The strain-specific spectral emission properties of LCPs may point to different non-PrP constituents of plaques in the various strains or may directly identify distinct supramolecular arrangements of PrP^{Sc} stacks. We tested the latter hypothesis using morphologically diverse amyloid fibrils assembled from chemically identical recombinant PrP monomers[24,25]. We generated fibrils of recombinant mouse full-length PrP (recPrP) using two different *in vitro* conversion methods[26,27] that start either from natively folded (preparation A) or from denatured recPrP (preparation B) and vary primarily in protein, salt and urea concentrations (**Supplementary Methods** online). Neither protocol included detergents or lipids that might have interfered with LCP binding. To exclude possible effects of pH or ionic strength on probe binding, we dialyzed each fibril preparation against water and diluted them to the same protein concentration before use in assays.

We confirmed the presence of fibrils by imaging thioflavin T fluorescence (**Fig. 4c**) and detecting them by electron microscopy (**Supplementary Fig. 4** online). At pH = 4.0, PTAA stained both recPrP fibril preparations A and B, and its emission spectrum unambiguously discriminated the two samples (**Fig. 4d**). The spectral differences were less pronounced in alkaline buffer systems at pH = 10.0, suggesting that the interaction between the fibrils and PTAA is partly electrostatic, and that LCP-exposed charges are different in fibrils A and B. PTMI staining of fibrils A and B also resulted in pronounced spectral differences (**Fig. 4e**). The spectrum of PTMI-stained fibrils B closely resembled that of PTMI-stained prion aggregates in tissue sections (data not shown). As fibrils A and B were generated using identical PrP monomers and the system was devoid of any other proteins or of lipids, the observed spectral differences of the LCPs are due to different high-order conformations of the fibrils A and B.

Staining of field TSE samples

We also tested whether LCPs can discriminate among different prion strains in field TSE cases. We stained formic acid–treated, formalin-fixed paraffin-embedded brain sections from deer CWD, sheep scrapie, BSE and bovine amyloidotic spongiform encephalopathy (BASE)[28] with PTAA and PTMI. BSE (n = 20) and BASE (n = 2) were reliably distinguished by differential staining with LCPs (**Fig. 5**). PrP aggregates of BSE were stained by PTMI but not by PTAA, whereas both LCPs stained BASE aggregates. Both PTAA and PTMI stained noncongophilic and thioflavin T^- PrP aggregates in deer CWD (n = 3) and sheep scrapie (n = 3). Hence LCPs augment the conventional techniques and could be used to distinguish different ruminant TSE strains (**Supplementary Table 4** online).

In CWD-affected deer brains, costaining of the same section with PrP antibody 34C9 and with PTAA resulted in colocalization of the PrP immunohistochemical and the LCP fluorescence signals (**Fig. 5a**). In contrast, PTAA reactivity of PrP aggregates in sections of scrapie-affected sheep brains was abrogated by pretreatment with antibody 34C9, suggesting that the antibody interfered with probe binding (**Fig. 5b**).

DISCUSSION

The biochemical techniques that have been developed for studying mammalian prion strains[5,7–9] suggest that the tertiary and/or quaternary structure of PrP aggregates is an important factor in

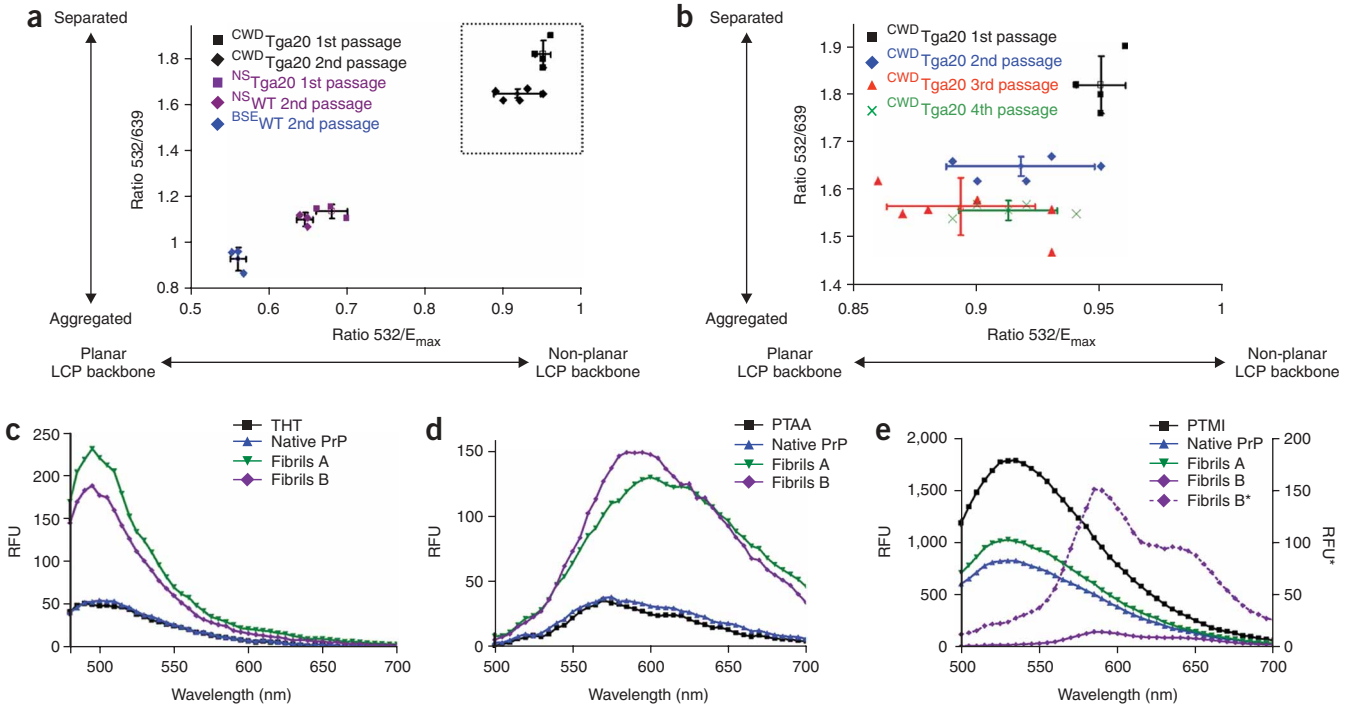

Figure 4 | Spectral data of mouse PrP deposits stained with PTAA and of recombinant mouse PrP fibrils stained by thioflavin T, PTAA or PTMI. (**a**,**b**) Correlation diagram of the ratios of emitted intensities, $R_{532/639}$ and $R_{532/Emax}$, of the intensity of the emitted light from PTAA bound to PrP plaques in individual ^{NS}tga20, ^{CWD}tga20, ^{NS}WT and ^{BSE}WT. The image in **b** is an expansion of the marked region in **a**, and depicts four passages of CWD in tga20 mice. (**c**–**e**) Emission spectra of thioflavin T, PTMI and PTAA bound to native or fibrillar recombinant mouse PrP. B* in **e** identifies the spectral curve of preparation B plotted on a different scale (right *y* axis). RFU, relative fluorescence units.

specifying strain properties. However, it has proven difficult to substantiate this conjecture because only a few methods are available to detect conformational variations between different PrP aggregates in tissue[10]. Here we exploited the unique optophysical properties of LCPs to distinguish among prion strains propagated in mice with identical PrP allelotypes.

LCPs appear to bind preferentially to protein aggregates with repetitive cross–β-sheet structures[13], whereas other molecules physiologically present in brain are left unstained or emit light of clearly different colors. Not only did LCPs stain all amyloid deposits that were identified by thioflavin T and Congo red stains, but they also identified noncongophilic aggregates in ^{RML}tga20 ($PTMI^+$) and ^{NS}WT ($PTAA^+$) brain samples as well as in brain samples from cattle, sheep and deer with naturally occurring prion disease. These noncongophilic LCP^+ aggregates were composed of PrP, as shown by SAF84 immunological reactivity. This could mean that LCP fluorescence yields stronger signals than thioflavin T and Congo red birefringence, resulting in higher sensitivity and detection of deposits that would have gone undetected with other amyloidotropic methods. Alternatively, the range of aggregate topologies identified by LCPs may include a subset of those stainable by thioflavin T or Congo red as well as deposits not formally qualifying as amyloid. Whether the LCP staining of noncongophilic deposits is due to higher sensitivity or to fundamental differences in the biophysical nature of the detected PrP^{Sc} deposits, it is highly specific: it was restricted to prion-infected organisms and to deposits that are stained by anti-PrP.

Changes in LCP geometry, owing to the relative orientation of thiophene rings within the polymer backbones and between polymer chains, translate into altered intensity of emitted light at given wavelengths. The latter can be visualized by spectral analyses and are often evident by fluorescence microscopy[12–15]. Such changes can occur upon binding to aggregated proteins[12,13], thereby providing a link between spectral signature and protein conformation. Therefore, the strain-specific spectroscopic signatures generated by the interaction of PTAA with PrP^{Sc} deposits may yield insights into the structural basis of prion strains.

We achieved additional discrimination by varying the functional side chains of the LCPs used for histochemical stains, with PrP^{Sc} deposits being stained by specific combinations of LCPs in a strain-specific manner. By combining the differential reactivity to chemically unique LCP variants with fluorescent spectral analysis, we achieved robust discrimination among at least four distinct prion strains propagated in mice.

Whereas prion strains faithfully maintain their phenotype over serial passages in congenic hosts, in many instances the incubation time of disease is progressively shortened and the attack rate becomes progressively higher. This phenomenon has been termed strain adaptation. More abrupt changes in strain phenotypes were termed strain mutations[29]. Therefore, strains, rather than being indefinitely stable, possess a certain degree of plasticity and can be modulated—to some extent, and over prolonged periods—by the genetic makeup of their hosts.

The biophysical basis of strain adaptation and mutation is not well understood. Notably, we found that adaptation of ruminant prions to mice by serial passaging was accompanied by progressive changes in PTAA spectra, suggesting (i) that LCP spectra can be used to report the molecular changes underlying strain adaptation,

and (ii) that strain adaptation is brought about by gradual host-constrained changes in the supramolecular arrangement of PrP^{Sc} deposits. Therefore, LCP spectra appear to visualize subtle strain-dependent phenomena that are not, or not always, reflected in macroscopic phenotypes. This suggests that there is more to strains than is phenotypically visible.

What is the molecular nature of the strain-specific traits that are differentiated by LCP emission spectra? On the one hand, the phenomena visualized by LCP staining may directly reflect changes in the tertiary and/or quaternary structure of PrP aggregates. Alternatively, it is possible that the changes in the photophysical properties of PTAA and the differential binding of chemically distinct LCPs depends on ancillary molecules that may be associated with PrP^{Sc} deposits. Therefore, we investigated this question in a chemically well-defined paradigm. Fibrils generated with different protocols from identical recombinant PrP were found to give rise to different spectral shifts, similar to those observed in different tissue sections. This provides support to the notion that the observed spectral variations are due to differences in protein conformation.

As we demonstrated, LCPs can be used as an optical tool for distinguishing structural variants of PrP aggregates associated with distinct mouse-adapted prion strains. Besides their obvious

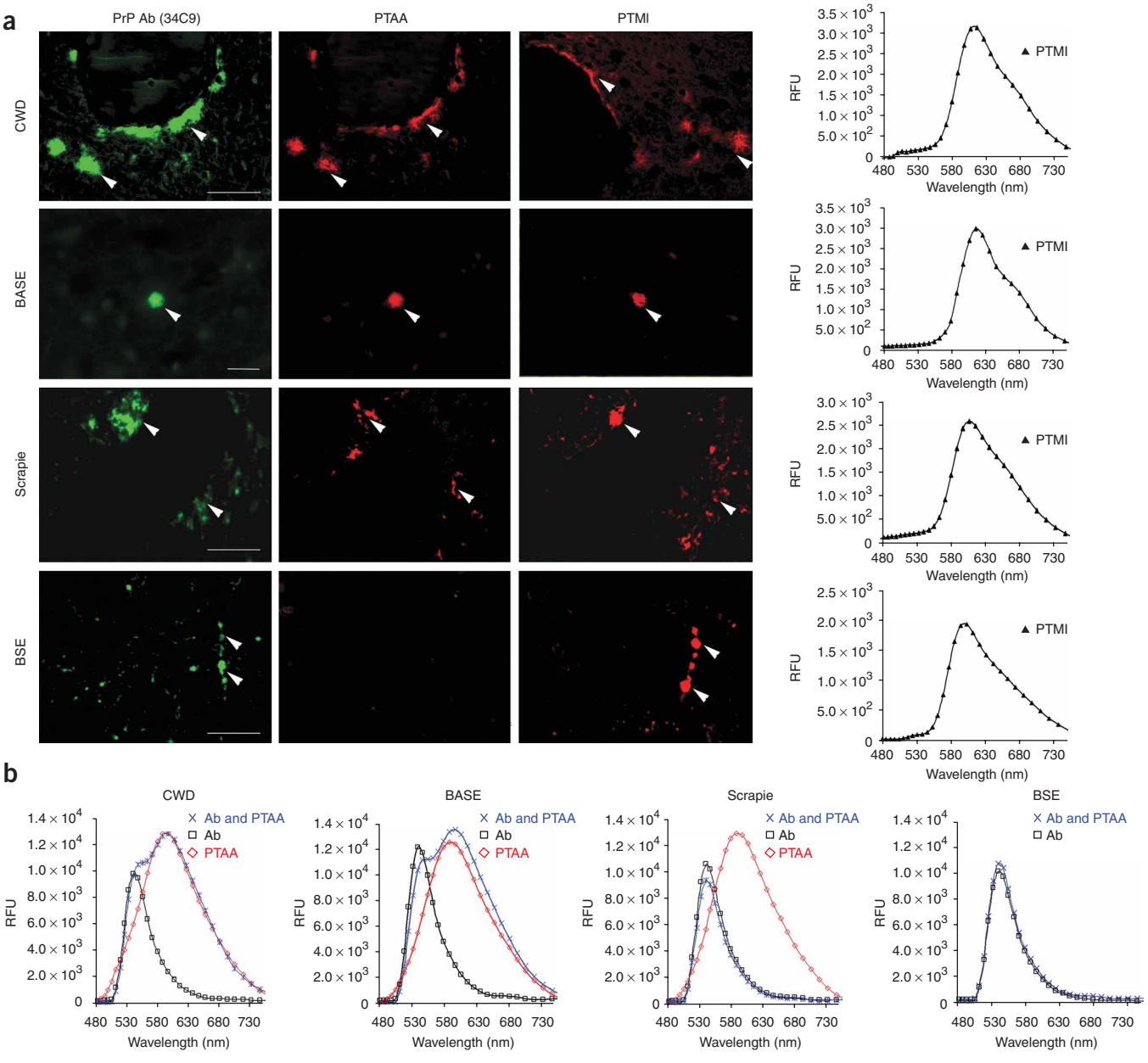

Figure 5 | LCP and PrP antibody stains of natural cases of BSE and BASE in cattle, CWD in mule deer and scrapie in sheep. (**a**) Formalin-fixed brain sections stained with anti-PrP 34C9, PTAA or PTMI. Only CWD, BASE and sheep scrapie cases were stained by PTAA, whereas all sections were stained by PTMI and anti-PrP 34C9. The staining was performed on the same section (PTAA, CWD and BASE) or adjacent sections (PTAA, BSE and sheep scrapie, all PTMI) and the spectra for PTMI bound to PrP-aggregates are shown on the right. Arrowheads indicate PrP aggregates. (**b**) Spectral analysis of PrP-aggregates showing anti-PrP 34C9 (Ab), PTAA and anti-PrP 34C9–PTAA costaining (Ab and PTAA). RFU, relative fluorescence units. Scale bars, 50 μm (**a**; CWD, scrapie, BSE) and 20 μm (**a**; BASE).

practical usefulness in diagnostic strain typing, LCP-based strain technologies should facilitate the understanding of the biophysical basis of prion strains. Phenomena similar to those occurring in prion strains may be much more frequent than is now appreciated, and may extend to additional protein misfolding and aggregation disorders. For example, strain-like conformational variants have been described for Aβ aggregation, which underlies Alzheimer's disease[30]. We therefore foresee that LCP-based techniques will aid in the fundamental understanding of conformational protein variants in a wide range of protein misfolding disorders.

METHODS

Prion inoculations. Tga20 transgenic mice, which overexpress mouse PrP[16], or wild-type mice were intracerebrally inoculated into the left parietal cortex with 30 µl of brain homogenate. This was either a 10% brain homogenate from a terminally sick, naturally CWD-infected mule deer ($n = 10$ mice), an uninfected control deer[17] ($n = 10$ mice), a 5% brain homogenate from an end-stage diseased, naturally scrapie-infected Suffolk sheep ($n = 4$ mice), or a 5% brain homogenate from a naturally BSE-infected cow ($n = 4$ mice). We monitored mice every second day and killed them at the onset of terminal scrapie. All experiments with mice were approved by the Swiss Veterinary Authorities.

Lesion profile. We selected 9–10 anatomic brain regions in accordance with previous strain-typing protocols[2,18] from 3–5 mice. We evaluated spongiosis on a scale of 0–4 (not detectable, mild, moderate, severe and status spongiosus). We scored gliosis and PrP immunological reactivity on a 0–3 scale (not detectable, mild, moderate, severe). A sum of the three scores resulted in the value obtained for the lesion profile for the individual animal. The 'radar plots' depict the scores for spongiform changes, gliosis and PrP deposition. Numbers correspond to the following brain regions: (1) dorsal medulla, (2) cerebellum, (3) hypothalamus, (4) medial thalamus, (5) hippocampus, (6) septum, (7) medial cerebral cortex dorsal to hippocampus, (8) medial cerebral cortex dorsal to septum, (9) white matter at cerebellar peduncles and (10) white matter at cerebral peduncles. Investigators blinded to animal identification performed histological analyses.

Western blots. We prepared 10% brain or spleen homogenates in PBS using a Ribolyzer (Hybaid). We diluted extracts of 50–90 µg protein with a Tris-based buffer (10 mM Tris, 10 mM EDTA, 100 mM NaCl, 0.5% Nonidet P-40 and 0.5% deoxycholate) and digested them with 100 µg/ml proteinase K for 30 min at 37 °C. Then we added SDS-based buffer and heated the samples to 95 °C for 5 min before electrophoresis through a 12% bis-Tris precast gel (Invitrogen), followed by transfer to a nitrocellulose membrane by wet blotting. Proteins were detected with the following 'POM' anti-PrP: POM1 (epitope in the globular domain, amino acids 121–230), POM12 (epitope on the octarepeats: amino acids 58–64, 66–72, 74–80, 82–88), POM3 (epitope at amino acids 95–100), and POM7 (epitope in the globular domain, amino acids 121–230)[6]. For secondary detection we used an HRP-conjugated anti-mouse immunoglobulin gamma (Zymed, Invitrogen). Signals were visualized with the ECL detection kit (Pierce).

LCP synthesis and LCP staining of tissue sections. The synthesis of PTAA (mean molecular weight, MW = 3 kDa) and PTMI (MW = 11 kDa) have been reported[19,20]. We dried 10-µm thick frozen mouse brain sections for 1 h and fixed them in 100% ethanol for 10 min. After washing with deionized water, we equilibrated the sections in incubation buffer solution, that is, 50 mM HCl at pH 1.6 (PTMI staining) or 100 mM sodium carbonate at pH 10.2 (PTAA staining). We diluted LCPs in incubation buffer (10 µg in 1,000 µl), added them to the brain sections, which were then incubated for 30 min at room temperature (18–22 °C) and washed with incubation buffer.

Paraffin-embedded formalin-fixed and formic-acid treated brain sections were de-paraffinized and treated with proteinase K (10 µg/ml in PBS) for 10 min before staining. We performed LCP staining as described above.

Fluorescence microscopy. We collected spectra with two different setups. For frozen sections, we recorded spectra with a LSM 510 META (Zeiss) confocal laser scanning microscope with a Plan-Neofluar 40L/0.75 objective. The sample was excited with a laser tuned to 488 nm and the emitted fluorescence was detected in steps of 10.7 nm by a photomultiplier tube array detector with 32 elements (META detector accessory). Accompanying software was used for the presentation of images and selection of spectral regions. Spectra were collected from 10 individual spots within 3–5 plaques from 19 mice with CWD, 3 mice with NS, 3 mice with ^{BSE}WT and 3 mice with ^{NS}WT.

For formalin-fixed paraffin sections, we recorded spectra with a Zeiss Axioplan 2 microscope, fitted with a Spectraview 4.0 (Applied Spectral Imaging) and a Spectra-Cube (interferometrical optical head SD 300) module with cooled charge-coupled device (CCD) camera, through a 405/30 nm (LP470) or a 470/40 nm (LP515) bandpass filter. The data were processed with SpectraView 3.0 EXPO. We collected spectra from PrP antibody– or LCP-stained PrP aggregates (8 individual spots for each sample) and other fluorescent entities in 5 mice with BSE, 3 mice with CWD, 3 mice with sheep scrapie and 2 mice with BASE. Fluorescent spectral unmixing was performed using the function in the software. As the BSE-infected mouse samples stained by PTAA were negative, we used the spectra recorded for PrP-aggregates in samples from mice infected with CWD and sheep scrapie for spectral unmixing analysis.

Additional methods. Detailed methods for the conformational stability assay, co-staining of tissue sections using anti-PrP and LCPs, fibril preparation and statistical methods, as well as two protocols for LCP staining in tissue cryosections and formalin-fixed, paraffin-embedded tissue sections are available in **Supplementary Methods**.

Note: Supplementary information is available on the Nature Methods website.

ACKNOWLEDGMENTS

This study was supported by grants from the European Union (Tseur to A.A. and Understanding Protein Misfolding and Aggregation by NMR (UPMAN) to K.W.), the Swiss National Science Foundation, the Swiss National Competence Centers for Research on Neural Plasticity and Repair (A.A.) and on Structural Biology (K.W.), US National Institutes of Health K08-AI01802 (C.J.S.), the Foundation for Research at the University of Zürich (C.J.S.), the US National Prion Research Program (C.J.S. and A.A.), the Knut and Alice Wallenberg foundation (K.P.R.N.), the Swedish Foundation for Strategic Research (P.H.), the Wenner-Gren Foundations and the Swedish Research Council (P.H.), and the Natural Sciences and Engineering Research Council of Canada (M.L.). We thank P. Vilkman, S. Fransson and C. von Schroetter for providing technical support, P. Tittmann (Electron

Microscopy Center, ETH Zurich) for providing electron microscopy services, the staff at the confocal microscopy centers at the ETH Zurich and at the University of Zurich for help with spectral collection, B. Seifert for help with statistical analysis, and C. Casalone (Istituto Zooprofilattico Sperimentale del Piemonte), F. Ehrensperger (University of Zürich), M. Miller (Colorado Division of Wildlife) and K. O'Rourke (United States Department of Agriculture) for BASE, BSE, CWD and sheep scrapie brain samples, respectively.

COMPETING INTERESTS STATEMENT

The authors declare competing financial interests: details accompany the full-text HTML version of the paper at http://www.nature.com/naturemethods/.

Published online at http://www.nature.com/naturemethods
Reprints and permissions information is available online at http://npg.nature.com/reprintsandpermissions

1. Prusiner, S.B. Novel proteinaceous infectious particles cause scrapie. *Science* **216**, 136–144 (1982).
2. Fraser, H. & Dickinson, A.G. The sequential development of the brain lesion of scrapie in three strains of mice. *J. Comp. Pathol.* **78**, 301–311 (1968).
3. Fraser, H. & Dickinson, A.G. Scrapie in mice. Agent-strain differences in the distribution and intensity of grey matter vacuolation. *J. Comp. Pathol.* **83**, 29–40 (1973).
4. Bruce, M.E., McBride, P.A. & Farquhar, C.F. Precise targeting of the pathology of the sialoglycoprotein, PrP, and vacuolar degeneration in mouse scrapie. *Neurosci. Lett.* **102**, 1–6 (1989).
5. Bessen, R.A. & Marsh, R.F. Biochemical and physical properties of the prion protein from two strains of the transmissible mink encephalopathy agent. *J. Virol.* **66**, 2096–2101 (1992).
6. Polymenidou, M. *et al.* Coexistence of multiple PrPSc types in individuals with Creutzfeldt-Jakob disease. *Lancet Neurol.* **4**, 805–814 (2005).
7. Hill, A.F. *et al.* Distinct glycoform ratios of protease resistant prion protein associated with PRNP point mutations. *Brain* **129**, 676–685 (2006).
8. Safar, J. *et al.* Eight prion strains have PrP(Sc) molecules with different conformations. *Nat. Med.* **4**, 1157–1165 (1998).
9. Peretz, D. *et al.* A change in the conformation of prions accompanies the emergence of a new prion strain. *Neuron* **34**, 921–932 (2002).
10. Aguzzi, A. Understanding the diversity of prions. *Nat. Cell Biol.* **6**, 290–292 (2004).
11. Weissmann, C. A 'unified theory' of prion propagation. *Nature* **352**, 679–683 (1991).
12. Nilsson, K.P.R., Herland, A., Hammarstrom, P. & Inganas, O. Conjugated polyelectrolytes: conformation-sensitive optical probes for detection of amyloid fibril formation. *Biochemistry* **44**, 3718–3724 (2005).
13. Nilsson, K.P.R. *et al.* Conjugated polyelectrolytes-conformation-sensitive optical probes for staining and characterization of amyloid deposits. *ChemBioChem* **7**, 1096–1104 (2006).
14. Nilsson, K.P., Rydberg, J., Baltzer, L. & Inganas, O. Self-assembly of synthetic peptides control conformation and optical properties of a zwitterionic polythiophene derivative. *Proc. Natl. Acad. Sci. USA* **100**, 10170–10174 (2003).
15. Nilsson, K.P.R., Rydberg, J., Baltzer, L. & Inganas, O. Twisting macromolecular chains: self-assembly of a chiral supermolecule from nonchiral polythiophene polyanions and random-coil synthetic peptides. *Proc. Natl. Acad. Sci. USA* **101**, 11197–11202 (2004).
16. Fischer, M. *et al.* Prion protein (PrP) with amino-proximal deletions restoring susceptibility of PrP knockout mice to scrapie. *EMBO J.* **15**, 1255–1264 (1996).
17. Sigurdson, C.J. *et al.* Strain fidelity of chronic wasting disease upon murine adaptation. *J. Virol.* **80**, 12303–12311 (2006).
18. Bruce, M.E., McConnell, I., Fraser, H. & Dickinson, A.G. The disease characteristics of different strains of scrapie in Sinc congenic mouse lines: implications for the nature of the agent and host control of pathogenesis. *J. Gen. Virol.* **72**, 595–603 (1991).
19. Ding, L., Jonforsen, M., Roman, L.S., Andersson, M.R. & Inganas, O. Photovoltaic cells with a conjugated polyelectrolyte. *Synth. Met.* **110**, 133–140 (2000).
20. Ho, H.-A. *et al.* Colorimetric and fluorometric detection of nucleic acids using cationic polythiophene derivatives. *Angew. Chem. Int. Edn. Engl.* **41**, 1548–1551 (2002).
21. Andersson, M.R. *et al.* Improved photoluminescence efficiency of films from conjugated polymers. *Synth. Met.* **85**, 1383–1384 (1997).
22. Berggren, M. *et al.* Controlling inter-chain and intra-chain excitations of a poly(thiophene) derivative in thin films. *Chem. Phys. Lett.* **304**, 84–90 (1999).
23. Nilsson, K.P.R., Andersson, M.R. & Inganas, O. Conformational transitions of a free amino-acid-functionalized polythiophene induced by different buffer systems. *J. Phys. Condens. Matter* **14**, 10011–10020 (2002).
24. Petkova, A.T. *et al.* Self-propagating, molecular-level polymorphism in Alzheimer's beta-amyloid fibrils. *Science* **307**, 262–265 (2005).
25. Jimenez, J.L. *et al.* The protofilament structure of insulin amyloid fibrils. *Proc. Natl. Acad. Sci. USA* **99**, 9196–9201 (2002).
26. Apetri, A.C., Vanik, D.L. & Surewicz, W.K. Polymorphism at residue 129 modulates the conformational conversion of the D178N variant of human prion protein 90–231. *Biochemistry* **44**, 15880–15888 (2005).
27. Bocharova, O.V., Breydo, L., Parfenov, A.S., Salnikov, V.V. & Baskakov, I.V. *In vitro* conversion of full-length mammalian prion protein produces amyloid form with physical properties of PrP(Sc). *J. Mol. Biol.* **346**, 645–659 (2005).
28. Casalone, C. *et al.* Identification of a second bovine amyloidotic spongiform encephalopathy: molecular similarities with sporadic Creutzfeldt-Jakob disease. *Proc. Natl. Acad. Sci. USA* **101**, 3065–3070 (2004).
29. Asante, E.A. *et al.* BSE prions propagate as either variant CJD-like or sporadic CJD-like prion strains in transgenic mice expressing human prion protein. *EMBO J.* **21**, 6358–6366 (2002).
30. Meyer-Luehmann, M. *et al.* Exogenous induction of cerebral beta-amyloidogenesis is governed by agent and host. *Science* **313**, 1781–1784 (2006).